

**SARS-CoV-2 Omicron BA.2.12.1, BA.4, and BA.5 subvariants  
evolved to extend antibody evasion**

Qian Wang<sup>1\*</sup>, Yicheng Guo<sup>1\*</sup>, Sho Iketani<sup>1,2</sup>, Zhiteng Li<sup>1</sup>, Hiroshi Mohri<sup>1</sup>, Maple Wang<sup>1</sup>, Jian Yu<sup>1</sup>, Anthony D. Bowen<sup>1,3</sup>, Jennifer Y. Chang<sup>3</sup>, Jayesh G. Shah<sup>3</sup>, Nadia Nguyen<sup>1</sup>, Kathrine Meyers<sup>1,3</sup>, Michael T. Yin<sup>1,3</sup>, Magdalena E. Sobieszczyk<sup>1,3</sup>, Zizhang Sheng<sup>1</sup>, Yaoxing Huang<sup>1</sup>, Lihong Liu<sup>1#</sup>, and David D. Ho<sup>1,2,3#</sup>

<sup>1</sup>Aaron Diamond AIDS Research Center, Columbia University Vagelos College of Physicians and Surgeons, New York, NY, USA.

<sup>2</sup>Department of Microbiology and Immunology, Columbia University Vagelos College of Physicians and Surgeons, New York, NY, USA.

<sup>3</sup>Division of Infectious Diseases, Department of Medicine, Columbia University Vagelos College of Physicians and Surgeons, New York, NY, USA.

\*Equal contribution

#Address correspondence to Lihong Liu ([ll3411@cumc.columbia.edu](mailto:ll3411@cumc.columbia.edu)) or David D. Ho ([dh2994@cumc.columbia.edu](mailto:dh2994@cumc.columbia.edu)), Columbia University Vagelos College of Physicians and Surgeons, 701 W. 168<sup>th</sup> Street, New York, NY 10032, USA.

## 1 **Abstract**

2 The Omicron subvariant BA.2 accounts for a large majority of the SARS-CoV-2 infection  
3 worldwide today<sup>1</sup>. However, its recent descendants BA.2.12.1 and BA.4/5 have surged  
4 dramatically to become dominant in the United States and South Africa, respectively<sup>2,3</sup>. That these  
5 novel Omicron subvariants carry additional mutations in their spike proteins raises concerns that  
6 they may further evade neutralizing antibodies, thereby further compromising the efficacy of our  
7 COVID-19 vaccines and therapeutic monoclonals. We now report findings from a systematic  
8 antigenic analysis of these surging Omicron subvariants. BA.2.12.1 is only modestly (1.8-fold)  
9 more resistant to sera from vaccinated and boosted individuals than BA.2. On the other hand,  
10 BA.4/5 is substantially (4.2-fold) more resistant and thus more likely to lead to vaccine  
11 breakthrough infections. Mutation at spike residue L452 found in both BA.2.12.1 and BA.4/5  
12 facilitates escape from some antibodies directed to the so-called Class 2 and Class 3 regions of the  
13 receptor-binding domain (RBD)<sup>4</sup>. The F486V mutation found in BA.4/5 facilitates escape from  
14 certain Class 1 and Class 2 antibodies to the RBD but compromises the spike affinity for the  
15 cellular receptor ACE2. The R493Q reversion mutation, however, restores receptor affinity and  
16 consequently the fitness of BA.4/5. Among therapeutic antibodies authorized for clinical use, only  
17 bebtelovimab (LY-COV1404) retains full potency against both BA.2.12.1 and BA.4/5. The  
18 Omicron lineage of SARS-CoV-2 continues to evolve, successively yielding subvariants that are  
19 not only more transmissible but also more evasive to antibodies.

20

21

22

23

24

25

26

27

28

29

## 30 **Main text**

31 SARS-CoV-2 Omicron (B.1.1.529) variant continues to dominate the COVID-19 pandemic.  
32 Globally, the BA.2 subvariant has rapidly replaced previous subvariants BA.1 and BA.1.1 (Fig.  
33 1a). The recent detection and dramatic expansion of three new Omicron subvariants have raised  
34 concerns. BA.2.12.1 emerged in the United States in early February and expanded substantially  
35 in the northeast region that includes New York (Fig. 1a), where it now accounts for over 70% of  
36 all new SARS-CoV-2 infections<sup>3</sup>. BA.4 and BA.5 emerged in South Africa in January and rapidly  
37 became dominant there with a combined frequency of over 88%<sup>1</sup>. These new Omicron subvariants  
38 have been detected worldwide, albeit at low levels presently. However, their growth trajectories  
39 in the U.S. and South Africa indicate a significant transmission advantage that will likely result in  
40 further expansion, as is being observed in countries such as Portugal (Fig. 1a). Phylogenetically,  
41 these new subvariants evolved independently from BA.2 (Fig. 1b). The spike protein of BA.2.12.1  
42 contains L452Q and S704L alterations in addition to the known mutations in BA.2, whereas the  
43 spike proteins of BA.4 and BA.5 are identical, each with four additional alterations: Del69-70,  
44 L452R, F486V, and R493Q, a reversion mutation (Fig. 1c). The location of several of these  
45 mutations within RBD of the spike protein (Extended Data Fig. 1) raises the specter that BA.2.12.1  
46 and BA.4/5 may have evolved to further escape from neutralizing antibodies.

47

## 48 **Neutralization by monoclonal antibodies**

49 To understand antigenic differences of BA.2.12.1 and BA.4/5 from previous Omicron subvariants  
50 (BA.1, BA.1.1, and BA.2) and the wild-type SARS-CoV-2 (D614G), we produced each  
51 pseudovirus and then assessed the sensitivity of each pseudovirus to neutralization by a panel of  
52 21 monoclonal antibodies (mAbs) directed to known neutralizing epitopes on the viral spike.  
53 Among these, 19 target the four epitope classes in RBD<sup>4</sup>, including REGN10987 (imdevimab)<sup>5</sup>,  
54 REGN10933 (casirivimab)<sup>5</sup>, COV2-2196 (tixagevimab)<sup>6</sup>, COV2-2130 (cilgavimab)<sup>6</sup>, LY-CoV555  
55 (bamlanivimab)<sup>7</sup>, CB6 (etesevimab)<sup>8</sup>, Brie-196 (amubarvimab)<sup>9</sup>, Brie-198 (romlusevimab)<sup>9</sup>, S309  
56 (sotrovimab)<sup>10</sup>, LY-CoV1404 (bebtelovimab)<sup>11</sup>, ADG-2<sup>12</sup>, DH1047<sup>13</sup>, S2X259<sup>14</sup>, CAB-A17<sup>15</sup> and  
57 ZCB11<sup>16</sup>, as well as 1-20, 2-15, 2-7<sup>17</sup> and 10-40<sup>18</sup> from our group. Two other mAbs, 4-18 and 5-  
58 7<sup>17</sup>, target the N-terminal domain (NTD). Our findings are shown in Fig. 2a, as well as in Extended  
59 Data Figs. 2 & 3. Overall, 18 and 19 mAbs lost neutralizing activity completely or partially against  
60 BA.2.12.1 and BA.4/5, respectively. Neutralization profiles were similar for BA.2 and BA.2.12.1

61 except for three Class 3 RBD mAbs (Brii-198, REGN10987, and COV2-2130) that were either  
62 inactive or further impaired against the latter subvariant. Compared to BA.2 and BA.2.12.1,  
63 BA.4/5 showed substantially greater neutralization resistance to two Class 2 RBD mAbs (ZCB11  
64 and COV2-2196) as well as modest resistance to two Class 3 RBD mAbs (REGN10987 and  
65 COV2-2130). Collectively, these differences suggest that mutations in BA.2.12.1 confer greater  
66 evasion from antibodies to RBD Class 3 region, whereas mutations in BA.4/5 confer greater  
67 evasion from antibodies to RBD Class 2 and Class 3 regions. Only four mAbs (CAB-A17, COV2-  
68 2130, 2-7, and LY-COV1404) retained good in vitro potency against both BA.2.12.1 and BA.4/5  
69 with IC<sub>50</sub> below 0.1 µg/mL. Importantly, among these four mAbs, only LY-COV1404 or  
70 bebtelovimab is authorized for therapeutic use in the clinic. For antibody combinations previously  
71 authorized or approved for clinical use, all showed a substantial loss of activity in vitro against  
72 BA.2.12.1 and BA.4/5.

73  
74 To identify the mutations in BA.2.12.1 and BA.4/5 that confer antibody resistance, we assessed  
75 the neutralization sensitivity of pseudoviruses carrying each of the point mutations in the  
76 background of D614G or BA.2 to the aforementioned panel of mAbs and combinations. Detailed  
77 findings are presented in Extended Data Figs. 4-6, and most salient results are highlighted in Fig.  
78 2b and discussed here. Substitutions (M, R, and Q) at residue L452, previously found in the Delta  
79 and Lambda variants<sup>19,20</sup>, conferred resistance largely to Classes 2 and 3 RBD mAbs, with L452R  
80 being the more detrimental mutation. F486V broadly impaired the neutralizing activity of several  
81 Class 1 and Class 2 RBD mAbs. Notably, this mutation decreased the potency of ZCB11 by  
82 >2000-fold. In contrast, the reversion mutation R493Q sensitized BA.2 to neutralization by  
83 several Class 1 and Class 2 RBD mAbs. This finding is consistent with our previous study<sup>21</sup>  
84 showing that Q493R found in the earlier Omicron subvariants mediated resistance to the same set  
85 of mAbs. L452, F486, and Q493, situated at the top of RBD, are among the residues most  
86 commonly targeted by SARS-CoV-2 neutralizing mAbs whose epitopes have been defined (Fig.  
87 2c). In silico structural analysis showed that both L452R and L452Q caused steric hindrance to  
88 the binding by Class 2 RBD mAbs. One such example is shown for LY-CoV555 (Fig. 2d),  
89 demonstrating the greater clash because of the Arginine substitution and explaining why this  
90 particular mutation led to a larger loss of virus-neutralizing activity (Fig. 2b). Structural modeling

91 of the F486V again revealed steric hindrance to binding by Class 2 RBD mAbs such as  
92 REGN10933, LY-CoV555, and 2-15 caused by the Valine substitution (Fig. 2e).

93

#### 94 **Affinity to human ACE2**

95 Epidemiological data clearly indicate that both BA.2.12.1 and BA.4/5 are very transmissible (Fig.  
96 1a); however, the additional mutations at the top of RBD (Fig. 2c) of these subvariants raises the  
97 possibility of a significant loss of affinity for the viral receptor, human ACE2 (hACE2), as has  
98 been reported by one group<sup>22</sup>. We therefore measured the binding affinity of purified spike  
99 proteins of D614G and major Omicron subvariants (Extended Data Fig. 7) to dimeric hACE2 using  
100 surface plasmon resonance (SPR). The spike proteins of the Omicron subvariants exhibited similar  
101 binding affinities to hACE2, with  $K_D$  values ranging from 1.66 nM for BA.4/5 to 2.36 nM for  
102 BA.2.12.1 to 2.79 nM for BA.1.1 (Fig. 3a). Impressively, despite having  $\geq 17$  mutations in the  
103 RBD to escape antibody neutralization, BA.2.12.1 and BA.4/5 also evolved concurrently to gain  
104 a slightly higher affinity for the receptor than an ancestral SARS-CoV-2, D614G ( $K_D$  5.20 nM).

105

106 To support the findings by SPR and to probe the role of point mutations in hACE2 binding, we  
107 tested BA.2, BA.2.12.1, and BA.4/5 pseudoviruses, as well as pseudoviruses containing key  
108 mutations, to neutralization by dimeric hACE2 in vitro. The  $IC_{50}$  values were lower for BA.4/5  
109 and BA.2.12.1 than that of BA.2 (Fig. 3b), again indicating that these two emerging Omicron  
110 subvariants have not lost receptor affinity. Our results also showed that the F486V mutation  
111 compromised receptor affinity, as previously reported<sup>23</sup>, while the R493Q reversion mutation  
112 improved receptor affinity. To structurally interpret these results, we modeled F486V and R493Q  
113 mutations based on the crystal structure of BA.1-RBD-hACE2 complex<sup>24</sup> overlaid with ligand-  
114 free BA.2 RBD (PDB: 7U0N and 7UB0). This analysis found that both R493 and F486 are  
115 conformationally similar between BA.1 and BA.2, and F486V led to a loss of interaction with a  
116 hydrophobic pocket in hACE2 (Fig. 3c). On the other hand, the R493Q reversion mutation  
117 restored a hydrogen bond with H34 and avoided the charge repulsion by K31, seemingly having  
118 the opposite effect of F486V. Interestingly, the mutation frequency at F486 had been exceedingly  
119 low ( $< 10E-5$ ) until the emergence of BA.4/5 (Extended Data Table 1), probably because of a  
120 compromised receptor affinity. Taken together, our findings in Figs. 2 and 3 suggest that F486V

121 allowed BA.4 and BA.5 to extend antibody evasion while R493Q compensated for their fitness  
122 loss.

123

### 124 **Neutralization by polyclonal sera**

125 We next assessed the extent of BA.2.12.1 and BA.4/5 resistance to neutralization by sera from  
126 four different clinical cohorts. Sera from persons immunized with only two doses of COVID-19  
127 mRNA vaccines were not examined because most of them could not neutralize earlier Omicron  
128 subvariants<sup>21,25</sup>. Instead, we measured serum neutralizing activity for persons who received three  
129 shots of mRNA vaccines (boosted), individuals who received mRNA vaccines before or after non-  
130 Omicron infection, and patients with either BA.1 or BA.2 breakthrough infection after vaccination.  
131 Their clinical information is described in Extended Data Table 2, and the serum neutralization  
132 profiles are presented in Extended Data Fig. 8 and the 50% inhibitory dose (ID<sub>50</sub>) titers are  
133 summarized in Fig. 4a. For the “boosted” cohort, neutralization titers were noticeably lower (4.6-  
134 fold to 6.2-fold) for BA.1, BA.1.1, and BA.2 compared to D614G (Fig. 4b), as previously  
135 reported<sup>21,25</sup>. Titers for BA.2.12.1 and BA.4/5 were even lower, by 8.1-fold and 19.2-fold,  
136 respectively, relative to D614G, and by 1.8-fold and 4.2-fold, respectively, relative to BA.2. A  
137 similar trend was observed for serum neutralization for the other cohorts, with the lowest titers  
138 against BA.4/5, followed next by titers against BA.2.12.1. Relative to BA.2, BA.2.12.1 and  
139 BA.4/5 showed 1.2-fold to 1.4-fold and 1.6-fold to 4.3-fold, respectively, greater resistance to  
140 neutralization by sera from these individuals who had both mRNA vaccination and SARS-CoV-2  
141 infection.

142

143 We also conducted serum neutralization assays on pseudoviruses containing point mutations found  
144 in BA.2.12.1 or BA.4/5 in the background of BA.2. Del69-70, L452M/R/Q, and F486V each  
145 modestly (1.1-fold to 2.4-fold) decreased the neutralizing activity of sera from all cohorts, while  
146 the R493Q reversion mutation modestly (~1.5-fold) enhanced the neutralization (Fig. 4c and  
147 Extended Data Fig. 9). S704L, a mutation close to the S1/S2 cleavage site, did not appreciably  
148 alter the serum neutralization titers against BA.2. For “boosted” serum samples, the impact of  
149 each point mutant on neutralization resistance was quantified and summarized in Fig. 4b.

150

151 Using these serum neutralization results, we then constructed a graphic display to map antigenic  
152 distances among D614G, various Omicron subvariants, and individual point mutants for just the  
153 “boosted” samples to avoid confounding effects from differences in clinical histories in the other  
154 cohorts. The resultant antigenic cartography (Fig. 4d) shows that BA.1, BA.1.1, and BA.2 are  
155 approximately equidistant from D614G, with each about 3-4 antigenic units away. BA.2.12.1 is  
156 further away from BA.2 by 1 antigenic unit. Most strikingly, BA.4/5 is 6 antigenic units from the  
157 D614G and 4 antigenic units from BA.2. Each of the point mutants Del69-70, L452M/Q/R, and  
158 F486V adds antigenic distance from BA.2 and D614G, whereas R493Q has the opposite effect.  
159 Overall, this map makes clear that BA.4/5 is substantially more neutralization resistant to sera  
160 obtained from vaccinated and boosted individuals, with several mutations contributing to the  
161 antibody evasion.

162

## 163 **Discussion**

164 We have systematically evaluated the antigenic properties of SARS-CoV-2 Omicron subvariants  
165 BA.2.12.1 and BA.4/5, which are rapidly expanding in the United States and South Africa,  
166 respectively (Fig. 1a). It is apparent that BA.2.12.1 is only modestly (1.8-fold) more resistant to  
167 sera from vaccinated and boosted individuals than the BA.2 subvariant that currently dominates  
168 the global pandemic (Figs. 4b). On the other hand, BA.4/5 is substantially (4.2-fold) more resistant,  
169 a finding consistent with results recently posted by other groups<sup>2,26</sup>. This antigenic distance is  
170 similar to that between the Delta variant and the ancestral virus<sup>27</sup> and thus is likely to lead to more  
171 breakthrough infections in the coming months. A key question now is whether BA.4/5 would out-  
172 compete BA.2.12.1, which poses less of an antigenic threat. The answer should be forthcoming  
173 soon in “battlegrounds” where both subvariants are already present and expanding, such as New  
174 York. Epidemiologically, since both of these two Omicron subvariants have a clear advantage in  
175 transmission, it is therefore not surprising that their abilities to bind the hACE2 receptor remain  
176 robust (Fig. 3a) despite numerous mutations in the spike protein. In fact, BA.4/5 may have slightly  
177 higher affinity for the receptor, contrary to suggestions that it might be less fit<sup>22</sup>.

178

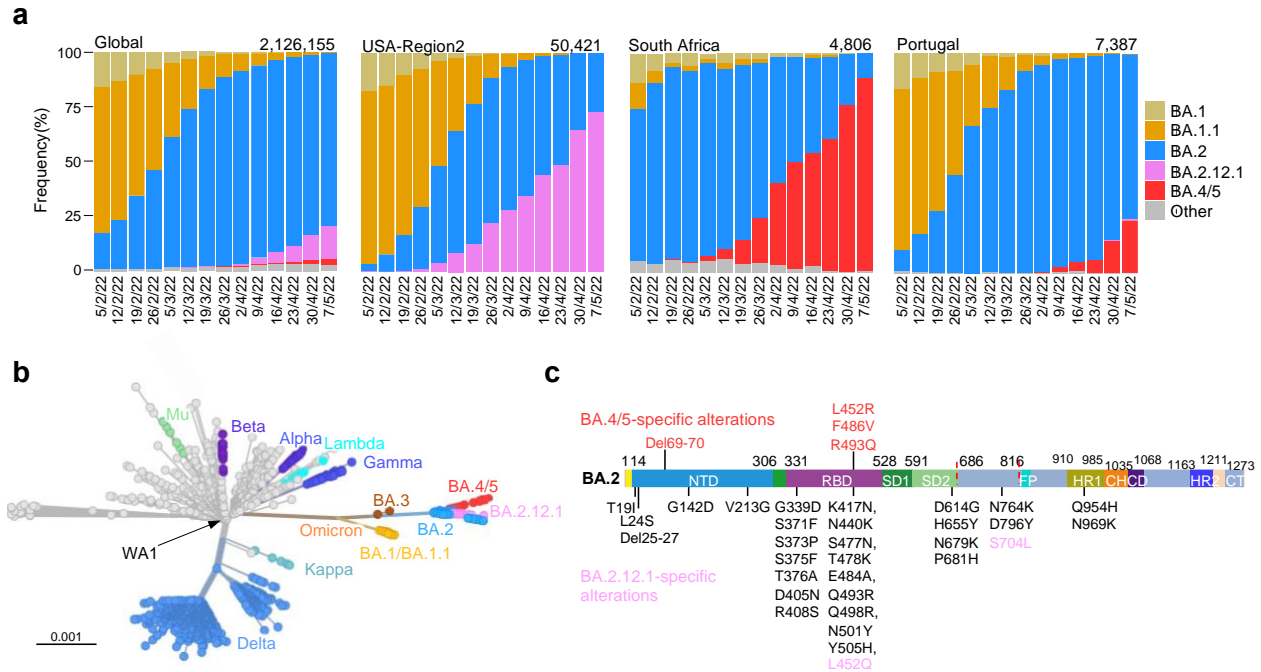
179 Our studies on the specific mutations found in BA.2.12.1 and BA.4/5 show that Del69-70,  
180 L452M/R/Q, and F486V could individually contribute to antibody resistance, whereas R493Q

181 confers antibody sensitivity (Fig. 4b). Moreover, the data generated using SARS-CoV-2-  
182 neutralizing mAbs suggest that a mutation at L452 allows escape from Class 2 and Class 3 RBD  
183 antibodies and that the F486V mutation mediates escape from Class 1 and Class 2 RBD antibodies  
184 (Fig. 2b). It is not clear how Del69-70, a mutation previously seen in the Alpha variant<sup>28</sup>,  
185 contributes to antibody resistance except for the possible evasion from certain neutralizing  
186 antibodies directed to the NTD. As for the use of clinically authorized mAbs to treat or block  
187 infection by BA.2.12.1 or BA.4/5, only bebtelovimab (LY-COV1404)<sup>11</sup> retains exquisite potency  
188 while the combination of tixagevimab and cilgavimab (COV2-2196 and COV2-2130)<sup>6</sup> shows a  
189 modest loss of activity (Fig. 2a).

190

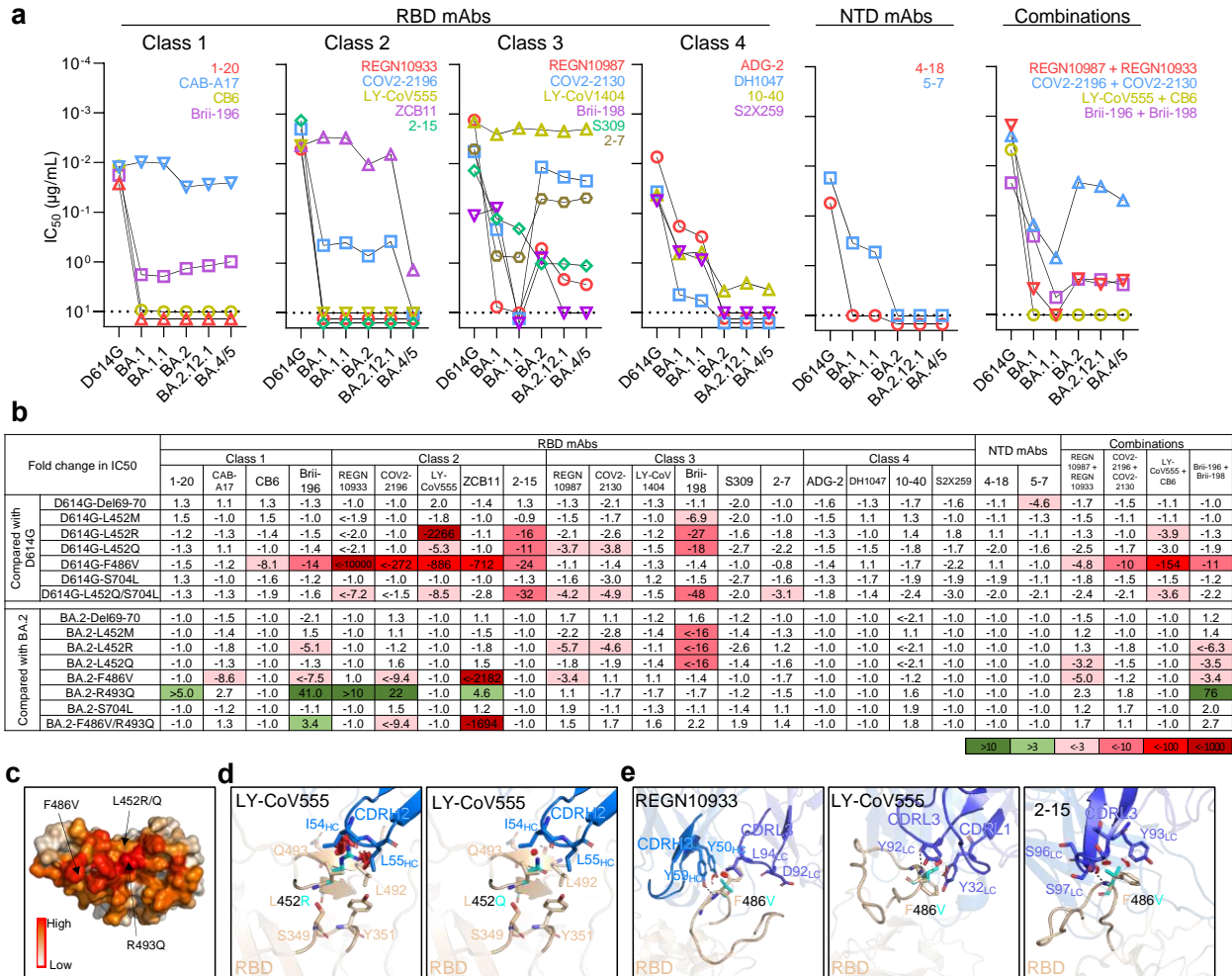
191 As the Omicron lineage has evolved over the past few months (Fig. 1b), each successive subvariant  
192 has seemingly become better and better at human transmission (Fig. 1a) as well as in antibody  
193 evasion<sup>21,29</sup>. It is only natural that scientific attention remains intently focused on each new  
194 subvariant of Omicron. However, we must be mindful that each of the globally dominant variants  
195 of SARS-CoV-2 (Alpha, Delta, and Omicron) emerged stochastically and unexpectedly.  
196 Vigilance in our collective surveillance effort must be sustained.





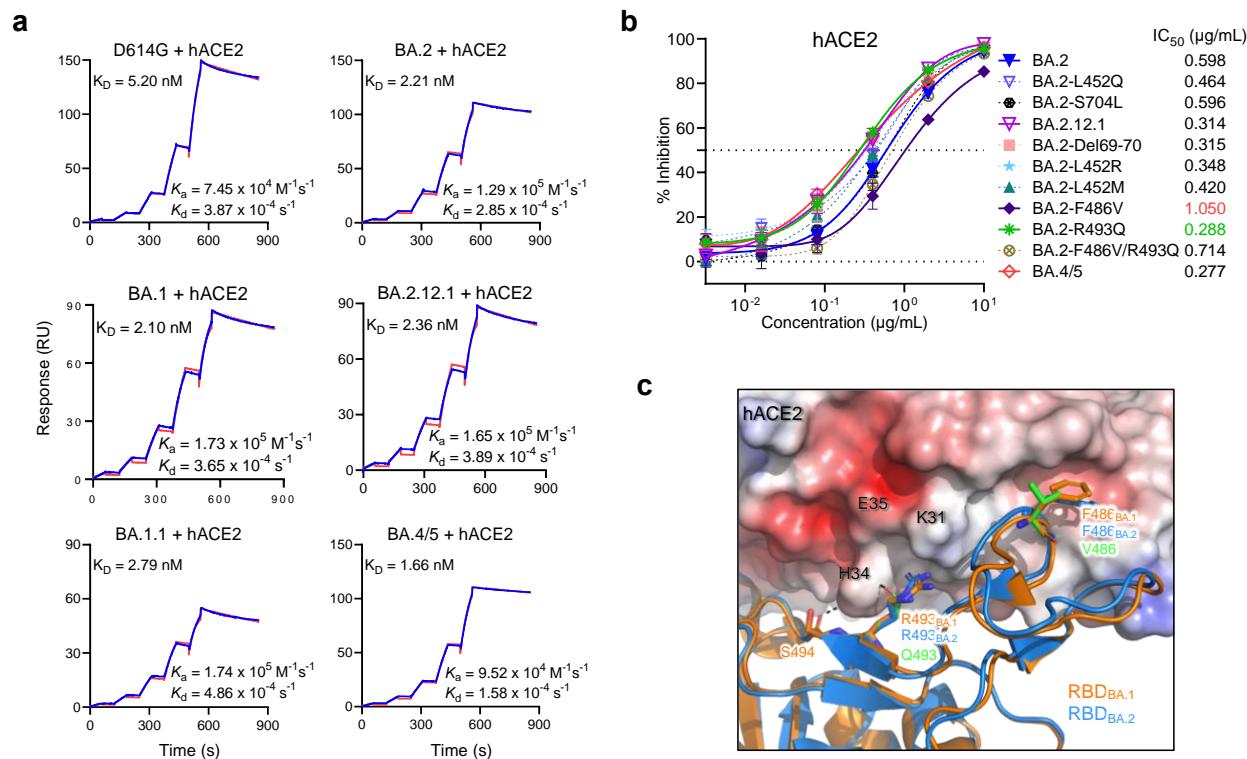
197

198 **Fig. 1 | Prevalence of SARS-CoV-2 Omicron sublineages.** **a**, Frequencies of BA.1, BA.1.1,  
 199 BA.2, BA.2.12.1, and BA.4/5 deposited in GISAID. The value in the upper right corner of each  
 200 box denotes the cumulative number of sequences for all circulating viruses in this time period. The  
 201 USA-Region2 is defined by the U.S. Department of Health & Human Service, including New  
 202 York, New Jersey, Puerto Rico and the Virgin Islands. **b**, Unrooted phylogenetic tree of Omicron  
 203 and its sublineages along with other major SARS-CoV-2 variants. **c**, Key spike mutations found  
 204 in BA.2, BA.2.12.1, BA.4, and BA.5. Del, deletion.



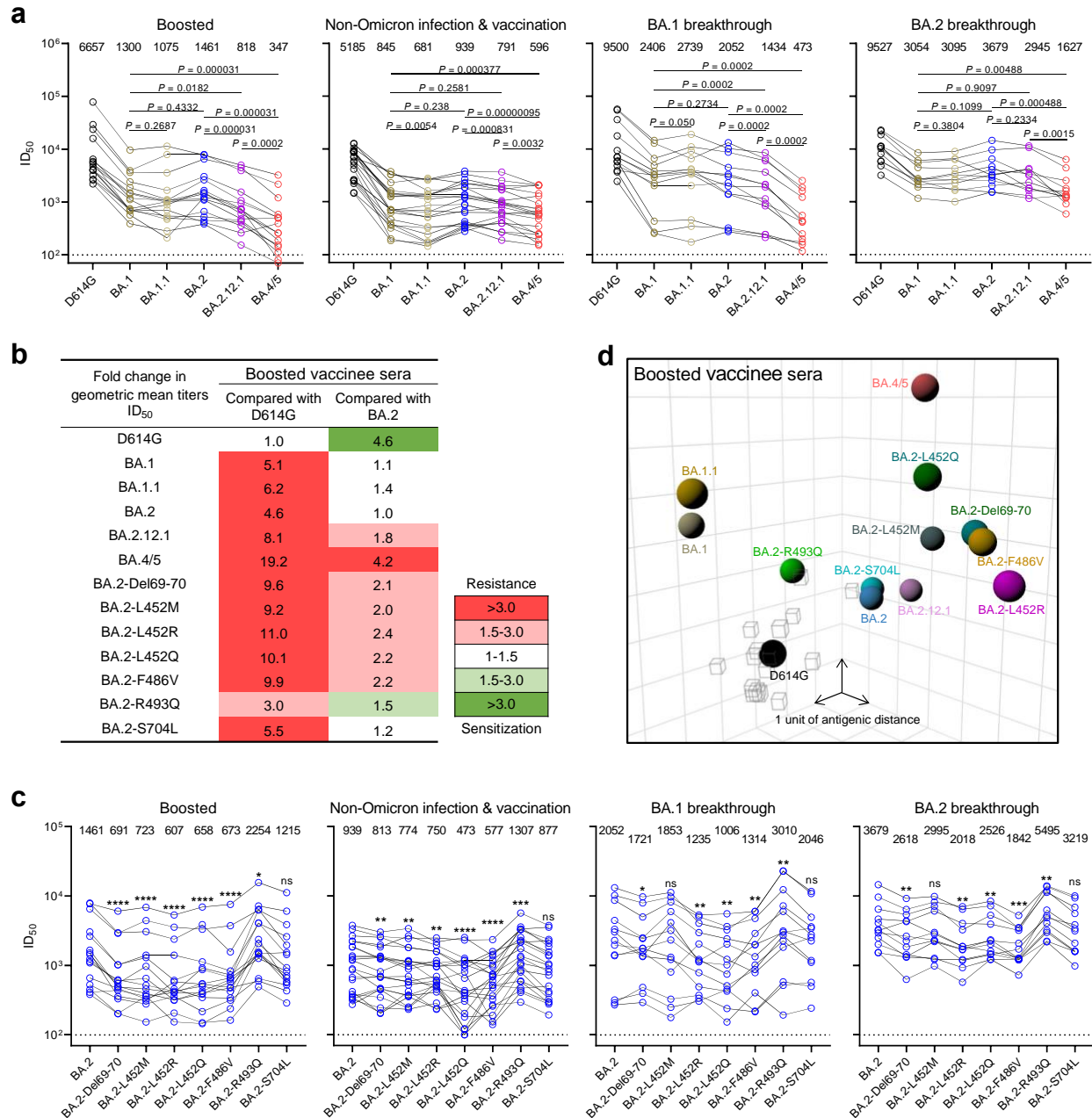
205

206 **Fig. 2 | Resistance of Omicron sublineages to neutralization by monoclonal antibodies.** a,  
 207 Neutralization of D614G and Omicron sublineages by RBD- and NTD-directed monoclonal  
 208 antibodies (mAbs). Values above the LOD of 10 µg/mL (dotted line) are arbitrarily plotted to allow  
 209 for visualization of each sample. b, Fold change in IC<sub>50</sub> values of point mutants relative to D614G  
 210 or BA.2, with resistance colored red and sensitization colored green. c, Location of F486V,  
 211 L452R/Q, and R493Q on D614G RBD, with the color indicating the per residue frequency  
 212 recognized by SARS-CoV-2 neutralizing antibodies. Modeling of L452R/Q (d) and F486V (e)  
 213 affect class 2 antibody neutralization. The clashes are shown in red plates; the hydrogen bonds are  
 214 shown in dark dashed lines.



215

216 **Fig. 3 | Affinity of the spike proteins of SARS-CoV-2 Omicron sublineages to human ACE2**  
 217 **(hACE2).** **a**, Binding affinities of Omicron subvariant S2P spike proteins to hACE2 as measured  
 218 by SPR. **b**, Sensitivity of pseudotyped Omicron sublineages and the individual mutations in the  
 219 background of BA.2 to hACE2 inhibition. The hACE2 concentrations resulting in 50% inhibition  
 220 of infectivity (IC<sub>50</sub>) are presented. Data are shown as mean ± SEM. **c**, In silico analysis for how  
 221 R493Q and F486V affect hACE2 binding. The hACE2 surface is shown with charge potential,  
 222 with red and blue representing negative and positive charges, respectively. Omicron BA.1 RBD in  
 223 complex with hACE2 was downloaded from PDB 7U0N, and the ligand-free BA.2 RBD was  
 224 downloaded from PDB 7UB0.



225

226 **Fig. 4 | BA.2.12.1 and BA.4/5 exhibit greater serum neutralization resistance profiles relative**  
 227 **to BA.2.** **a**, Neutralization of pseudotyped D614G and Omicron subvariants by sera from 4  
 228 different clinical cohorts. **b**, Fold change in geometric mean ID<sub>50</sub> titers of boosted vaccinee sera  
 229 relative to D614G and BA.2, with resistance colored red and sensitization colored green. **c**, Serum  
 230 neutralization of BA.2 pseudoviruses containing single mutations found within BA.2.12.1 and  
 231 BA.4/5. For all the panels, values above the symbols denote the geometric mean ID<sub>50</sub> values.

232 *P* values were determined by using two-tailed Wilcoxon matched-pairs signed-rank tests. \**p* <  
233 0.05, \*\**p* < 0.01; \*\*\**p* < 0.001; \*\*\*\**p* < 0.0001; ns - not significant. **d**, Antigenic map based on  
234 the neutralization data of boosted vaccinee sera and an interactive map is available online  
235 (<https://figshare.com/articles/media/OmicronAntigenicMap/19854046>).

## 236 References

- 237 1 Shu, Y. & McCauley, J. GISAID: Global initiative on sharing all influenza data - from vision to  
238 reality. *Euro Surveill* **22**, doi:10.2807/1560-7917.ES.2017.22.13.30494 (2017).
- 239 2 Khan, K. *et al.* Omicron sub-lineages BA.4/BA.5 escape BA.1 infection elicited neutralizing  
240 immunity. *medRxiv*, doi:10.1101/2022.04.29.22274477 (2022).
- 241 3 Centers for Disease Control and Prevention. *COVID Data Tracker*, <[https://covid.cdc.gov/covid-](https://covid.cdc.gov/covid-data-tracker/#variant-proportions)  
242 [data-tracker/#variant-proportions](https://covid.cdc.gov/covid-data-tracker/#variant-proportions)> (2022).
- 243 4 Barnes, C. O. *et al.* SARS-CoV-2 neutralizing antibody structures inform therapeutic strategies.  
244 *Nature* **588**, 682-687, doi:10.1038/s41586-020-2852-1 (2020).
- 245 5 Hansen, J. *et al.* Studies in humanized mice and convalescent humans yield a SARS-CoV-2  
246 antibody cocktail. *Science* **369**, 1010-1014, doi:10.1126/science.abd0827 (2020).
- 247 6 Zost, S. J. *et al.* Potently neutralizing and protective human antibodies against SARS-CoV-2.  
248 *Nature* **584**, 443-449, doi:10.1038/s41586-020-2548-6 (2020).
- 249 7 Jones, B. E. *et al.* The neutralizing antibody, LY-CoV555, protects against SARS-CoV-2 infection in  
250 nonhuman primates. *Sci Transl Med* **13**, doi:10.1126/scitranslmed.abf1906 (2021).
- 251 8 Shi, R. *et al.* A human neutralizing antibody targets the receptor-binding site of SARS-CoV-2.  
252 *Nature* **584**, 120-124, doi:10.1038/s41586-020-2381-y (2020).
- 253 9 Ju, B. *et al.* Human neutralizing antibodies elicited by SARS-CoV-2 infection. *Nature* **584**, 115-  
254 119, doi:10.1038/s41586-020-2380-z (2020).
- 255 10 Pinto, D. *et al.* Cross-neutralization of SARS-CoV-2 by a human monoclonal SARS-CoV antibody.  
256 *Nature* **583**, 290-295, doi:10.1038/s41586-020-2349-y (2020).
- 257 11 Westendorf, K. *et al.* LY-CoV1404 (bebtelovimab) potently neutralizes SARS-CoV-2 variants. *Cell*  
258 *Rep* **39**, 110812, doi:10.1016/j.celrep.2022.110812 (2022).
- 259 12 Rappazzo, C. G. *et al.* Broad and potent activity against SARS-like viruses by an engineered  
260 human monoclonal antibody. *Science* **371**, 823-829, doi:10.1126/science.abf4830 (2021).
- 261 13 Li, D. *et al.* In vitro and in vivo functions of SARS-CoV-2 infection-enhancing and neutralizing  
262 antibodies. *Cell* **184**, 4203-4219 e4232, doi:10.1016/j.cell.2021.06.021 (2021).
- 263 14 Tortorici, M. A. *et al.* Broad sarbecovirus neutralization by a human monoclonal antibody.  
264 *Nature* **597**, 103-108, doi:10.1038/s41586-021-03817-4 (2021).
- 265 15 Sheward, D. J. *et al.* Structural basis of Omicron neutralization by affinity-matured public  
266 antibodies. *bioRxiv*, doi:10.1101/2022.01.03.474825 (2022).
- 267 16 Zhou, B. *et al.* An elite broadly neutralizing antibody protects SARS-CoV-2 Omicron variant  
268 challenge. *bioRxiv*, doi:10.1101/2022.01.05.475037 (2022).
- 269 17 Liu, L. *et al.* Potent neutralizing antibodies against multiple epitopes on SARS-CoV-2 spike.  
270 *Nature* **584**, 450-456, doi:10.1038/s41586-020-2571-7 (2020).
- 271 18 Liu, L. *et al.* An antibody class with a common CDRH3 motif broadly neutralizes sarbecoviruses.  
272 *Sci Transl Med*, eabn6859, doi:10.1126/scitranslmed.abn6859 (2022).
- 273 19 Planas, D. *et al.* Reduced sensitivity of SARS-CoV-2 variant Delta to antibody neutralization.  
274 *Nature* **596**, 276-280, doi:10.1038/s41586-021-03777-9 (2021).
- 275 20 Kimura, I. *et al.* The SARS-CoV-2 Lambda variant exhibits enhanced infectivity and immune  
276 resistance. *Cell Rep* **38**, 110218, doi:10.1016/j.celrep.2021.110218 (2022).
- 277 21 Liu, L. *et al.* Striking antibody evasion manifested by the Omicron variant of SARS-CoV-2. *Nature*  
278 **602**, 676-681, doi:10.1038/s41586-021-04388-0 (2022).
- 279 22 Cao, Y. *et al.* BA.2.12.1, BA.4 and BA.5 escape antibodies elicited by Omicron infection. *bioRxiv*,  
280 doi:10.1101/2022.04.30.489997 (2022).
- 281 23 Starr, T. N. *et al.* Shifting mutational constraints in the SARS-CoV-2 receptor-binding domain  
282 during viral evolution. *bioRxiv*, doi:10.1101/2022.02.24.481899 (2022).

- 283 24 Geng, Q. *et al.* Structural Basis for Human Receptor Recognition by SARS-CoV-2 Omicron Variant  
284 BA.1. *J Virol* **96**, e0024922, doi:10.1128/jvi.00249-22 (2022).
- 285 25 Iketani, S. *et al.* Antibody evasion properties of SARS-CoV-2 Omicron sublineages. *Nature* **604**,  
286 553-556, doi:10.1038/s41586-022-04594-4 (2022).
- 287 26 Tuekprakhon, A. *et al.* Further antibody escape by Omicron BA.4 and BA.5 from vaccine and  
288 BA.1 serum. *bioRxiv*, doi:10.1101/2022.05.21.492554 (2022).
- 289 27 Rössler, A. *et al.* BA.2 omicron differs immunologically from both BA.1 omicron and pre-omicron  
290 variants. *medRxiv*, doi:10.1101/2022.05.10.22274906 (2022).
- 291 28 Wang, P. *et al.* Antibody resistance of SARS-CoV-2 variants B.1.351 and B.1.1.7. *Nature* **593**, 130-  
292 135, doi:10.1038/s41586-021-03398-2 (2021).
- 293 29 Yu, J. *et al.* Neutralization of the SARS-CoV-2 Omicron BA.1 and BA.2 Variants. *N Engl J Med* **386**,  
294 1579-1580, doi:10.1056/NEJMc2201849 (2022).
- 295 30 Wrapp, D. *et al.* Cryo-EM structure of the 2019-nCoV spike in the prefusion conformation.  
296 *Science* **367**, 1260-1263, doi:10.1126/science.abb2507 (2020).
- 297 31 Krissinel, E. & Henrick, K. Inference of macromolecular assemblies from crystalline state. *J Mol*  
298 *Biol* **372**, 774-797, doi:10.1016/j.jmb.2007.05.022 (2007).
- 299 32 Cerutti, G. *et al.* Structural basis for accommodation of emerging B.1.351 and B.1.1.7 variants by  
300 two potent SARS-CoV-2 neutralizing antibodies. *Structure* **29**, 655-663 e654,  
301 doi:10.1016/j.str.2021.05.014 (2021).
- 302 33 Smith, D. J. *et al.* Mapping the antigenic and genetic evolution of influenza virus. *Science* **305**,  
303 371-376, doi:10.1126/science.1097211 (2004).

304



305 **Methods**

306

307 **Data reporting**

308 No statistical methods were used to predetermine sample size. The experiments were not  
309 randomized and the investigators were not blinded to allocation during experiments and outcome  
310 assessment.

311

312 **Serum samples**

313 Sera from individuals who received three doses of the mRNA-1273 or BNT162b2 vaccine were  
314 collected at Columbia University Irving Medical Center. Sera from individuals who were infected  
315 by non-Omicron variants of SARS-CoV-2 in addition to vaccination were collected from January  
316 2021 to September 2021 at Columbia University Irving Medical Center or at the Hackensack  
317 Meridian Center for Discovery and Innovation (CDI). Sera from individuals who were infected by  
318 Omicron (BA.1 or BA.2) following vaccinations were collected from December 2021 to May 2022  
319 at Columbia University Irving Medical Center. All samples were confirmed for prior SARS-CoV-  
320 2 infection status by anti-nucleoprotein (NP) ELISA. All collections were conducted under  
321 protocols reviewed and approved by the Institutional Review Board of Columbia University or the  
322 Hackensack Meridian Center for Discovery and Innovation. All participants provided written  
323 informed consent. Clinical information on the different cohorts of study subjects is provided in  
324 Extended Data Table 2.

325

326 **Monoclonal antibodies**

327 Antibodies were expressed as previously described<sup>17</sup>. Heavy chain variable (VH) and light chain  
328 variable (VL) genes for each antibody were synthesized (GenScript), then transfected into Expi293  
329 cells (Thermo Fisher Scientific), and purified from the supernatant by affinity purification using  
330 rProtein A Sepharose (GE). REGN10987, REGN10933, COV2-2196, and COV2-2130 were  
331 provided by Regeneron Pharmaceuticals; Brie-196 and Brie-198 were provided by Brie Biosciences;  
332 CB6 was provided by B. Zhang and P. Kwong (NIH); and ZCB11 was provided by Z. Chen (HKU).

333

334 **Cell lines**



335 Expi293 cells were obtained from Thermo Fisher Scientific (A14527); Vero-E6 cells were  
336 obtained from the ATCC (CRL-1586); HEK293T cells were obtained from the ATCC (CRL-3216).  
337 Cells were purchased from authenticated vendors and morphology was confirmed visually before  
338 use. All cell lines tested mycoplasma negative.

339

### 340 **Variant SARS-CoV-2 spike plasmid construction**

341 BA.1, BA.1.1, and BA.2 spike-expressing plasmids were generated as previously described<sup>21,25</sup>.  
342 Plasmids encoding the BA.2.12.1 and BA.4/5 spikes, as well as the individual and double  
343 mutations found in BA.2.12.1 and BA.4/5, were generated using the QuikChange II XL site-  
344 directed mutagenesis kit according to the manufacturer's instructions (Agilent). To make the  
345 constructs for expression of stabilized soluble S2P spike trimer proteins, 2P substitutions (K986P  
346 and V987P) and a "GSAS" substitution of the furin cleavage site (682-685aa in WA1) were  
347 introduced into the spike-expressing plasmids<sup>30</sup>, and then the ectodomain (1-1208aa in WA1) of  
348 the spike was fused with a C-terminal 8x His-tag and cloned into the pAH vector. All constructs  
349 were confirmed by Sanger sequencing and the sequences of the oligos used are provided in  
350 Extended Data Table 3.

351

### 352 **Expression and purification of SARS-CoV-2 S2P spike proteins**

353 SARS-CoV-2 S2P spike trimer proteins of the D614G and Omicron subvariants were generated  
354 by transfecting Expi293 cells with the S2P spike trimer-expressing constructs using 1 mg mL<sup>-1</sup>  
355 polyethylenimine (PEI) and then purifying from the supernatants five days post-transfection using  
356 Ni-NTA resin (Invitrogen) according to the manufacturer's instructions<sup>17</sup>. Each S2P trimer protein  
357 (1.5 µg) was analyzed on a 4-12% NuPAGE™ Bis-Tris protein gel (Invitrogen) run at 200 V using  
358 MOPS buffer, after which the gel was stained with Coomassie Blue dye.

359

### 360 **Surface plasmon resonance**

361 Surface plasmon resonance (SPR) binding assays for human ACE2 binding to SARS-CoV-2 spike  
362 were performed using a Biacore T200 biosensor equipped with a Series S CM5 chip (Cytiva), in a  
363 running buffer of 10 mM HEPES pH 7.4, 150 mM NaCl, 3 mM EDTA, 0.05% P-20 (Cytiva) at  
364 25 °C. Spike proteins were captured through their C-terminal His-tag over an anti-His antibody  
365 surface. These surfaces were generated using the His-capture kit (Cytiva) according to the

366 manufacturer's instructions, resulting in approximately 10,000 RU of anti-His antibody over each  
367 surface. An anti-His antibody surface without antigen was used as a reference flow cell to remove  
368 bulk shift changes from the binding signal.

369 Binding of human ACE2-Fc protein (Sino Biological) was tested using a three-fold dilution  
370 series with concentrations ranging from 2.46 nM to 200 nM. The association and dissociation rates  
371 were each monitored for 60 s and 300 s respectively, at 30  $\mu\text{L}/\text{min}$ . The bound spike/ACE2  
372 complex was regenerated from the anti-His antibody surface using 10 mM glycine pH 1.5. Blank  
373 buffer cycles were performed by injecting running buffer instead of human ACE2-Fc to remove  
374 systematic noise from the binding signal. The resulting data was processed and fit to a 1:1 binding  
375 model using Biacore Evaluation Software.

376

### 377 **Pseudovirus production**

378 Pseudoviruses were produced in the vesicular stomatitis virus (VSV) background, in which the  
379 native glycoprotein was replaced by that of SARS-CoV-2 and its variants, as previously  
380 described<sup>17</sup>. In brief, HEK293T cells were transfected with a spike expression construct with 1 mg  
381  $\text{mL}^{-1}$  polyethylenimine (PEI) and cultured overnight at 37 °C under 5%  $\text{CO}_2$ , and then infected  
382 with VSV-G pseudotyped  $\Delta\text{G}$ -luciferase (G\* $\Delta\text{G}$ -luciferase, Kerafast) one day post-transfection.  
383 After 2 h of infection, cells were washed three times, changed to fresh medium, and then cultured  
384 for approximately another 24 h before the supernatants were collected, clarified by centrifugation,  
385 and aliquoted and stored at -80 °C for further use.

386

### 387 **Pseudovirus neutralization assay**

388 All viruses were first titrated to normalize the viral input between assays. Heat-inactivated sera or  
389 antibodies were first serially diluted in medium in 96-well plates in triplicate, starting at 1:100  
390 dilution for sera and 10  $\mu\text{g mL}^{-1}$  for antibodies. Pseudoviruses were then added and the virus–  
391 sample mixture was incubated at 37 °C for 1 h. Vero-E6 cells were then added at a density of  
392  $3 \times 10^4$  cells per well and the plates were incubated at 37 °C for approximately 10 h. Luciferase  
393 activity was quantified using the Luciferase Assay System (Promega) according to the  
394 manufacturer's instructions using SoftMax Pro v.7.0.2 (Molecular Devices). Neutralization curves  
395 and  $\text{IC}_{50}$  values were derived by fitting a nonlinear five-parameter dose–response curve to the data  
396 in GraphPad Prism v.9.2.

397

### 398 **Antibody targeting frequency and mutagenesis analysis for RBD**

399 The SARS-CoV-2 spike structure (6ZGE) used for displaying epitope footprints and mutations  
400 within the emerging variants was downloaded from the Protein Data Bank (PDB). Epitope residues  
401 were identified using PISA<sup>31</sup> with default parameters, and the RBD residues with non-zero buried  
402 accessible surface area were considered epitope residues. For each residue within the RBD, the  
403 frequency of antibody recognition was calculated as the number of contact antibodies<sup>32</sup>. The  
404 structures of antibody-spike complexes for modeling were also obtained from PDB (7L5B (2-15),  
405 6XDG (REGN10933), and 7KMG (LY-CoV555)). PyMOL v.2.3.2 was used to perform  
406 mutagenesis and to generate structural plots (Schrödinger).

407

### 408 **Antigenic cartography**

409 The antigenic distances between SARS-CoV-2 variants were approximated by incorporating the  
410 neutralization potency of each serum sample into a previously described antigenic cartography  
411 approach<sup>33</sup>. The map was generated by the Racmacs package (<https://acorg.github.io/Racmacs/>,  
412 version 1.1.4) in R with the optimization steps set to 2000, and with the minimum column basis  
413 parameter set to “none”.

414

415 **Acknowledgements**

416 This study was supported by funding from the Gates Foundation, JPB Foundation, Andrew and  
417 Peggy Cherng, Samuel Yin, Carol Ludwig, David and Roger Wu, Regeneron Pharmaceuticals,  
418 and the NIH SARS-CoV-2 Assessment of Viral Evolution (SAVE) Program. We acknowledge  
419 David S. Perlin for providing serum samples from a few COVID-19 patients.

420

421 **Author contributions**

422 D.D.H. and L.L. conceived this project. Q.W. and L.L. conducted pseudovirus neutralization  
423 experiments and purified SARS-CoV-2 spike proteins. Y.G. and Z.S. conducted bioinformatic  
424 analyses. Q.W., L.L., and S.I. constructed the spike expression plasmids. Q.W. managed the  
425 project. J.Y. and M.W. expressed and purified antibodies. L.L. and Z.L. performed surface  
426 plasmon resonance (SPR) assay. M.T.Y., M.E.S., J.Y.C., A.D.B. provided clinical samples. H.M.  
427 aided sample collections. Y.H. contributed to discussions. D.D.H. and L.L. directed and supervised  
428 the project. Q.W., Y.G., L.L., and D.D.H. analyzed the results and wrote the manuscript.

429

430 **Competing interests**

431 S.I, J.Y., Y.H., L.L., and D.D.H. are inventors on patent applications (WO2021236998) or  
432 provisional patent applications (63/271,627) filed by Columbia University for a number of SARS-  
433 CoV-2 neutralizing antibodies described in this manuscript. Both sets of applications are under  
434 review. D.D.H. is a co-founder of TaiMed Biologics and RenBio, consultant to WuXi Biologics  
435 and Brii Biosciences, and board director for Vicarious Surgical.

436

437 **Data and materials availability**

438 All data are provided in the manuscript.